Dynamic mechanisms for apparent slip on hydrophobic surfaces

Eric Lauga and Michael P. Brenner

Division of Engineering and Applied Sciences, Harvard University, 29 Oxford Street, Cambridge, Massachusetts 02138, USA
(Received 23 September 2003; revised manuscript received 22 March 2004; published 31 August 2004)

Recent experiments [Y. Zhu and S. Granick, Phys. Rev. Lett. **87**, 096105 (2001)] have measured a large, shear-dependent fluid slip at partially wetting fluid-solid surfaces. We present a simple model for such a slip, motivated by the recent observations of nanobubbles on hydrophobic surfaces. The model considers the dynamic response of bubbles to change in hydrodynamic pressure, due to the oscillation of a solid surface. Both the compression and diffusion of gas in the bubbles decrease the force on the oscillating surface by a "leaking mattress" effect, thereby creating an apparent shear-dependent slip. With bubbles similar to those observed by recent atomic force microscopy, the model predicts a force decrease consistent with the experimental measurements of Zhu and Granick.

I. INTRODUCTION

The validity of the no-slip boundary condition is at the center of our current understanding of fluid mechanics. It remains, however, an assumption whose microscopic validity has been widely debated [1]. The widespread acceptance of the no-slip condition is based on a historical record of outstanding agreement between theories and experiments. It is commonly agreed that the no-slip condition results from inevitable microscopic roughness, which causes enough viscous dissipation to effectively bring the fluid to rest near the surface [2–4]. Remarkably, this explanation is independent of the nature of the solid and the liquid, contrary to ideas first proposed by Girard (see Ref. [1]).

The development of small devices has recently prompted a reexamination of fluid slip on length scales of nanometers and micrometers, both experimentally [2,5–12] and theoretically [13–19]. The degree of slip is usually quantified by a slip length $\lambda = U_s / \dot{\gamma}$, where U_s is the slip velocity and $\dot{\gamma}$ is the liquid strain rate evaluated at the surface; equivalently, λ is the distance below the solid surface where the velocity extrapolates linearly to zero [20]. In experiments, slip is usually found when the liquid partially wets the solid surface; measured slip lengths span four orders of magnitude, from molecular sizes to micrometers, and are usually shear dependent in squeeze flow experiments, with λ an increasing function of $\dot{\gamma}$. In particular, Zhu and Granick [8] reported squeeze flow experiments, in which two crossed cylinders oscillate about a fixed average distance. By measuring the viscous resistance, Zhu and Granick extracted the slip length over a wide range of oscillation amplitudes. These experiments lead to the largest shear-dependent slip lengths yet (up to ~ 2 μm).

The origin of this large shear-dependent slip is heretofore mysterious. Nanobubbles have recently been observed on hydrophobic surfaces, using atomic force microscopy, with typical thickness $h \sim 10$ nm, typical radius $R \sim 50 - 100$ nm, and high surface coverage [21–24]. Although the origin of these bubbles is unclear and skepticism remains in the community about their existence, they have been often invoked as a possible origin of the so-called hydrophobic attraction

[25–29] and their existence points to a possible picture for such a large slip [19,22].

It is well known that there is in general a nonzero velocity at a liquid-gas interface, and therefore it is natural to wonder whether the existence of such a gas layer at the solid surface is sufficient to explain the experiments. When a fluid of viscosity η_1 adjoins a layer of fluid of thickness h with smaller viscosity η_2, the discontinuous strain rate at the fluid-fluid interface results in an apparent slip with slip length

$$\lambda = h \left(\frac{\eta_1}{\eta_2} - 1 \right). \tag{1}$$

Choosing $\eta_1 / \eta_2 = 50$ appropriate for a gas-water interface leads to slip lengths as large as 500 nm. This estimate is, however, independent of the interfacial shear and therefore unable to explain rate-dependent results from squeeze flow experiments; it also overestimates the slip length in the case of bubbles, as is discussed in Sec. III. Note, however, that similar arguments are consistent with data from pressure-driven flow experiments where reported slip lengths to date are essentially shear independent [10,11,18,30–32].

In this article, we will assume bubbles exist on hydrophobic surfaces and will calculate their *dynamic* response to an imposed oscillatory shear. In an oscillatory squeeze flow experiment [8], we argue that the pressure fluctuations in the fluid cause the bubbles to act as a "leaking mattress," with both the compression and the dilatation of the gas in the bubble, as well as the diffusion of gas into (and out of) the bubble. As the solid sphere oscillates, this periodic in-phase response of the bubbles sizes reduces the amount of liquid necessary to be squeezed out of the gap, and thereby the force on the moving sphere, creating an apparent slip. Our calculations indicate that the magnitude of this apparent slip is consistent with the observations of Zhu and Granick. We present the details of our model in the next section and discuss the comparison with the experiment in Sec. III.

II. INFLUENCE OF BUBBLES ON FORCE MEASUREMENTS

A typical oscillatory squeeze flow experiment is shown in Fig. 1. A sphere of radius a oscillates with velocity V_S in a
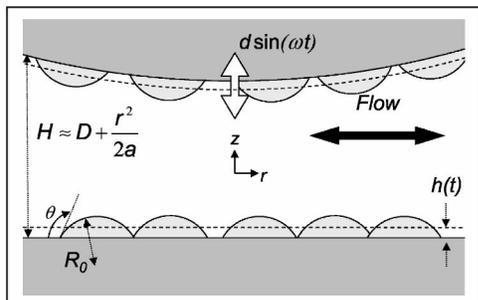
FIG. 1. A typical squeeze flow experiment: a solid sphere of radius a is oscillated in a liquid at a distance $D \ll a$ of a smooth solid surface with amplitude $d \ll D$ and frequency ω. The surfaces are covered by microscopic gas bubbles of contact angle θ and radius of curvature R_0. The set of bubbles is approximated by a gas layer of time evolving thickness $h(t)$.

viscous liquid of viscosity η at a distance D of a planar surface (equivalently, the surfaces can be two crossed cylinders). The two surfaces are assumed to have the same physicochemical properties. If no bubbles are present and the no-slip boundary condition is satisfied on both surfaces, then the lubrication force opposing the motion of the sphere is given by the Reynolds equation

$$F(t) = \mathbf{e}_z \cdot \mathbf{F}(t) = -\frac{6\pi\eta a^2}{D} V_S \triangleq F_{\text{lub}}. \tag{2}$$

If, however, flow occurs on the surfaces with a slip length λ, the viscous force is decreased by an amount f_{slip} [33] given by

$$f_{\text{slip}} = \frac{D}{3\lambda} \left[\left(1 + \frac{D}{6\lambda} \right) \ln \left(1 + \frac{6\lambda}{D} \right) - 1 \right]. \tag{3}$$

Equation (3) is used experimentally to infer effective slip lengths: the experimental viscous force F_{exp} is compared to the theoretical no-slip result F_{lub} and any difference is interpreted as fluid slip, with a slip length λ corresponding to $f_{\text{slip}} = F_{\text{exp}} / F_{\text{lub}}$.

Let us now *assume* that the solid surface is covered with a percentage ϕ of identical gas bubbles (Fig. 1), and determine how the bubbles modify the dynamic response. Although this assumption has been made by previous authors [19,22,26–29], the physical mechanism responsible for such bubbles is unknown. Simple estimates indicate that small bubbles are shortlived in solution [34]. However, stable bubbles could arise from any number of possibilities that are known to prolong bubble lifetimes, including surfactants, surface heterogeneities, or local supersaturation of dissolved gas [35]. In this paper, we are interested in understanding whether the dynamic response of hypothesized bubbles is sufficient to rationalize slip experiments.

A. Total force

The total force $F(t)$ resisting the oscillatory motion of the area S of the sphere has two components: (1) a viscous lubrication force F_h, due to hydrodynamic pressure fluctuations and acting on an area $(1-\phi)S$, and (2) an elastic bubble force

F_b, due to pressure fluctuations inside the bubbles and acting on an area ϕS. The total force is therefore given by

$$F(t) = (1-\phi)F_h + \phi F_b, \tag{4}$$

where

$$F_h = (p - p_0)S, \quad F_b = (p_b - p_{eq})S. \tag{5}$$

Here, p and p_b (p_0 and p_{eq}) denote the (equilibrium) pressures in the liquid and the bubbles, respectively. Moreover, since $D \ll a$, the surface S is given by $S \approx \pi a D$.

B. Lubrication force

Let us first calculate the hydrodynamic force F_h. The presence of bubbles modifies Eq. (2) in two ways. First, flow occurs over a distribution of bubbles located on an otherwise no-slip surface, so the viscous force is reduced by an amount f_{slip} given by Eq. (3), where λ is the appropriate effective slip length for flow over a distribution of bubbles [18,36].

Second, the size of the bubbles changes in time in response to pressure fluctuations in the liquid. This volume effect will modify the amount of liquid necessary to be squeezed out of the gap at each cycle of the oscillations, hence the viscous force. Consequently, bubble dynamics have to be subtracted from the forcing V_S and the hydrodynamic lubrication F_h force is now given by a modified Reynolds equation

$$F_h = -f_{\text{slip}} \frac{6\pi\eta a^2}{D} \left(V_S - 2\frac{dh}{dt} \right), \tag{6}$$

where h is an average bubble thickness on each surface and the factor 2 accounts for the fact that each surface is covered with bubbles.

C. Rate of change of bubble height

In order to calculate dh/dt in Eq. (6), let us now consider the dynamics of the bubbles. We assume the bubbles are undeformed by viscous stresses and remain spherical, with radius of curvature $R(t)$ and interior angle $(\pi - \theta)$ (see Fig. 1). We also neglect interactions between bubbles. We expect $h(t)$ to depend explicitly on the forcing on the bubbles, i.e. F_b.

At the small frequencies typical of squeeze flow experiments (1–100 Hz), the gas is isothermal, so the pressure in the bubble changes via the ideal gas law

$$\frac{p_b(t)V(t)}{m(t)} = \frac{p_{eq}V_0}{m_0}, \tag{7}$$

where V and m denote the volume and the mass of a single bubble. The average thickness of the gas layer is defined as $h(t) = nV(t)$, where n is the number density of bubbles on the solid surface, so that Eq. (7) can be rewritten as

$$\frac{p_b(t)h(t)}{m(t)} = \frac{p_{eq}h_0}{m_0}. \tag{8}$$

Combining the time derivative of Eq. (8) with $F_b = (p_b - p_{eq})S$ and linearizing around $\{p_b, h, m\} \sim \{p_{eq}, h_0, m_0\}$, we

obtain the equation for the rate of change of the mean bubble height h

$$\frac{\mathrm{d}h}{\mathrm{d}t} = \frac{h_0}{m_0}\frac{\mathrm{d}m}{\mathrm{d}t} - \frac{h_0}{p_{eq}S}\frac{\mathrm{d}F_b}{\mathrm{d}t}. \tag{9}$$

We thus have that the rate of change of h is the sum of a rate of change governed by gas diffusion, plus a second contribution due to the gas compressibility.

We now consider the rate of gas diffusion from the bubble. In our model for the oscillatory squeeze flow experiments [2,6,8], bubbles lose mass by both vertical diffusion across the liquid layer and radial diffusion along the apparatus; because of the scale separation $D \ll a$, these two processes require separate treatment.

Let us first consider the case of vertical diffusion. Since for most common gases, $\kappa \sim 10^{-9}$ m^2/s, the vertical Peclet number $\mathrm{Pe}_v = D^2\omega/\kappa$ is much smaller than unity: on the experimental time scale ω^{-1}, the bubbles are approximately in instantaneous vertical diffusive equilibrium. The dissolved gas concentration above the bubble is therefore uniform throughout the liquid gap and is given, in the case of small amplitude oscillations, by Henry's law $c = p_b c_\infty/p_{eq}$, where c_∞ is the far-field dissolved gas concentration. The mass $\tilde{m}$ of gas necessary to fill the liquid gap at this concentration is equal to the gap thickness $(D-2h)$, times the change in concentration $c_\infty(p_b/p_{eq}-1)$, times the area in the liquid that is influenced by the bubble, i.e. $1/n$. Linearizing around $h \approx h_0$ and combining with $p_{eq}/c_\infty = p_0/c_0$, we get that $\tilde{m}$ is proportional to the bubble force F_b:

$$\tilde{m} = \frac{c_0(D-2h_0)}{np_0S}F_b. \tag{10}$$

Consequently, the total rate of change of m is given by

$$\frac{\mathrm{d}m}{\mathrm{d}t} = \frac{\mathrm{d}m_r}{\mathrm{d}t} - \frac{c_0(D-2h_0)}{np_0S}\frac{\mathrm{d}F_b}{\mathrm{d}t}, \tag{11}$$

where $\mathrm{d}m_r/\mathrm{d}t$ is the rate of change in the bubble mass governed by gas diffusion in the (slowly varying) radial direction of the apparatus; let us now evaluate this contribution.

In contrast to the vertical case, the radial oscillatory Peclet number, $\mathrm{Pe}_r = L^2\omega/\kappa = aD\omega/\kappa$, is of order unity or larger, so that radial diffusion has to be accounted for explicitly. Assuming the dissolved gas is in vertical diffusive equilibrium, the time rate of change of the mass of a gas bubble $\mathrm{d}m_r/\mathrm{d}t$ is given by a flux integral on the bubble surface S_b,

$$\frac{\mathrm{d}m_r}{\mathrm{d}t} = \kappa \int_{S_b} \mathbf{n}\cdot\nabla c\,\mathrm{d}S = \kappa R^2 I(\theta)\frac{\partial c}{\partial r}, \tag{12}$$

where the assumption of the spherical cap bubble implies that $I(\theta) = \pi[2(\pi-\theta)+\sin 2\theta]/2$.

In general, the radial concentration of dissolved gas $c(r,t)$ verifies an advection-diffusion equation with shear-dependent diffusivity [37]. However, for the small amplitude oscillation in Ref. [8], both advection and Taylor dispersion are negligible, and $c(r,t)$ satisfies a pure diffusion equation. We finally approximate the radial concentration gradient by a simple linear law $\partial c/\partial r \approx (c_\infty - c)/L_r$, where $L_r \approx (\kappa/\omega)^{1/2}$

$\approx L/\mathrm{Pe}_r^{1/2}$ is the typical (shear-dependent) radial gradient length scale. Equation (12), together with Henry's law, leads, therefore, to a linear relation between the rate of change $\dot{m}_r$ and the bubble force

$$\frac{\mathrm{d}m_r}{\mathrm{d}t} = -\frac{\kappa R_0^2 I(\theta)c_0}{p_0 S L_r}F_b. \tag{13}$$

Combining $m_0 = \rho_0 h_0/n$ with Eqs. (9), (11), and (13), we finally obtain the result that the mean bubble height h satisfies the differential equation

$$\frac{\mathrm{d}h}{\mathrm{d}t} = -k_1 F_b - k_2\frac{\mathrm{d}F_b}{\mathrm{d}t}, \tag{14}$$

where (k_1,k_2) are given by

$$k_1 = \frac{n\kappa R_0^2 I(\theta)c_0}{\rho_0 p_0 S L_r}, \tag{15}$$

$$k_2 = \frac{c_0 h_0}{c_\infty p_0 S}\left(1 + \frac{c_\infty(D-2h_0)}{\rho_0 h_0}\right). \tag{16}$$

D. Bubble force

We finally need to calculate the bubble force F_b in order to close the system of equations (6) and (14). This, in general, requires understanding the (equilibrium or nonequilibrium) mechanism responsible for the presence of these long-lived bubbles. However, we can bypass this unknown physics by assuming without loss of generality that the pressure fluctuations in the bubbles and in the liquid are proportional

$$\Delta p_b = \alpha\,\Delta p, \tag{17}$$

where α is an unknown constant. Hence, bubble and hydrodynamic forces are proportional $F_b = \alpha F_h$, and the total force on the sphere can be expressed as

$$F = (1-\phi+\alpha\phi)\,F_h = \left(\frac{1-\phi+\alpha\phi}{\alpha}\right)F_b. \tag{18}$$

E. Total force on the sphere

We can now combine Eqs. (6), (14), and (18) to express the total force opposing the motion of the sphere F. We obtain

$$F(t) = -\frac{\delta}{2}(1-\phi+\alpha\phi)\left(V_S + 2k_1 F_b + 2k_2\frac{\mathrm{d}F_b}{\mathrm{d}t}\right), \tag{19}$$

where $\delta = 12\pi\eta a^2 f_{\mathrm{slip}}/D$. Since F and F_b are related by Eq. (18), Eq. (19) can be transformed into an ordinary differential equation for F,

$$F(t) = -\frac{\delta}{2}\left(\widetilde{V_S} + 2\alpha k_1 F + 2\alpha k_2\frac{\mathrm{d}F}{\mathrm{d}t}\right), \tag{20}$$

where $\widetilde{V_S} = (1-\phi+\alpha\phi)V_S$. For an oscillating sphere velocity $V_S = \mathrm{d}(d\sin\omega t)/\mathrm{d}t$, the periodic solution to Eq. (20) is given by [44]

TABLE I. Summary of experimental data on nanobubbles as found in Refs. [21–24] by atomic force microscopy: projected area of each bubble on the solid surfaces, height above the surfaces h_0, radius of curvature R_0, surface coverage ϕ, and macroscopic and microscopic contact angle. The radius of curvature and microscopic contact angles were inferred from the other data assuming spherical cap nanobubbles.

	Ishida *et al.* [21]	Tyrrell and Attard [22]	Tyrrell and Attard [23]	Steitz *et al.* [24]
Projected area (nm^2)	3.3×10^5	4–6×10^3	4–7×10^3	2–11×10^3
Height h_0 (nm)	40	20–30	20–30	<18
Radius of curvature R_0 (nm)	1300	~50	40–60	30–100
Surface coverage ϕ	~20%	~100%	~100%	89%
Macroscopic contact angle	110°	101°	101°	>90°
Microscopic contact angle θ	166°	~120°	117°–130°	130°–147°

$$\frac{F(t)}{F_{\text{lub}}} = f_{\text{slip}} \frac{(1 - \phi + \alpha\phi)(1 - \delta\alpha k_1)}{(1 + \delta\alpha k_1)^2 + (\delta\omega\alpha k_2)^2} \Bigg(\cos \omega t$$
$$+ \frac{\delta\omega\alpha k_2}{1 + \delta\alpha k_1} \sin \omega t \Bigg). \tag{21}$$

F. What is the value of α?

By comparing our model (21) to the results of squeeze flow experiments, we find that the only choice consistent with available data at large separation distances is $\alpha \approx 1$.

To see this, consider Eq. (21) in the limit of large separations between the sphere and the planar surface D. Since Eq. (3) shows that $f_{\text{slip}} \sim 1$ when D is large, we get $\delta \sim D^{-1}$. Moreover, $S \sim D$ so that, from Eqs. (15) and (16), we obtain $\delta k_1 \sim D^{-2}$ and $\delta k_2 \sim D^{-1}$. Consequently, in the limit of large separations, we obtain that the ratio of the measured force, out of phase with the sphere displacement, to the expected no-slip force (2) is given by

$$\lim_{D \to \infty} \left(\frac{F}{F_{\text{lub}}} \right) = 1 - \phi + \alpha\phi. \tag{22}$$

Within experimental errors, this ratio is always measured to be unity [2,7–9,12], i.e., the expected lubrication no-slip force is recovered for large separation distances. We therefore need $1 - \phi + \alpha\phi \approx 1$ or $\alpha \approx 1$. We emphasize that this conclusion is reached because we *assume* that the model presented in Sec. II is the major physical mechanism responsible for the force decrease observed in experiments such as in Ref. [8].

G. Final formula for the force ratio

We obtain from Eq. (21) that the ratio f^* of the peak force out of phase with the sphere displacement to that expected with no slip and no bubbles (2) is given by

$$\frac{f^*(\omega)}{f_{\text{slip}}} = \frac{1}{1 + \left(\delta k_1 + \dfrac{(\omega\delta k_2)^2}{1 + \delta k_1} \right)}. \tag{23}$$

The "leaking mattress" model therefore leads to an apparent slip effect, of dynamic origin. The effect is shear dependent

through the frequency dependence in Eq. (23): higher frequency and therefore higher shear rates lead to a larger apparent slip, in agreement with Refs. [2,7,8]. The model was derived under the assumption of small amplitude oscillations d, and consequently it does not appear in the final formula for f^*.

Equation (23) implies that the apparent slip effect increases with the fluid viscosity, in agreement with experiments [7,10]. It also increases with the size of the sphere a, which might account for the large slip lengths reported in Ref. [8] (centimeter-sized spheres) as opposed to other squeeze flow experiments (usually micrometer-sized spheres). The model predicts that the measured overall apparent slip length is therefore not only a solid/liquid property, but that it depends on the system size [18].

We finally note from Eq. (21) that the total pressure force on the sphere $F(t)$ also contains a nonzero component in phase with the displacement of the sphere, and therefore out of phase with its velocity. If we denote by g^* the ratio of this in-phase response to the expected no-slip no-bubbles out-of-phase response, we obtain

$$g^* = \frac{\delta\omega k_2}{(1 + \delta k_1)^2 + (\delta\omega k_2)^2} f_{\text{slip}} = \frac{\delta\omega k_2}{1 + \delta k_1} f^*. \tag{24}$$

Equation (24) is a prediction of the effective elasticity provided by the bubbles to the surface, which would occur in addition to other in-phase contributions such as intermolecular forces, and is experimentally testable. The values of the in-phase responses of the forces were unfortunately not reported by Zhu and Granick [8].

III. COMPARISON WITH EXPERIMENTS

We present in this section a quantitative comparison of our model with the experimental results of Zhu and Granick in the case of de-ionized water, namely the four sets of data presented in Fig. 2 of Ref. [8]. The macroscopic water/solid contact angle in this case was 110°, the sphere radius was $a = 2$ cm, and we assumed that the liquid was saturated with O_2 at 25 °C and 1 atm ($c_\infty = c_0$), for which $\rho_0 = 1.28$ kg/m^3, $c_0 = 8.3 \times 10^{-3}$ kg/m^3 and $\kappa = 2 \times 10^{-9}$ m^2/s. As a matter of comparison, we have also summarized in Table I the experi-
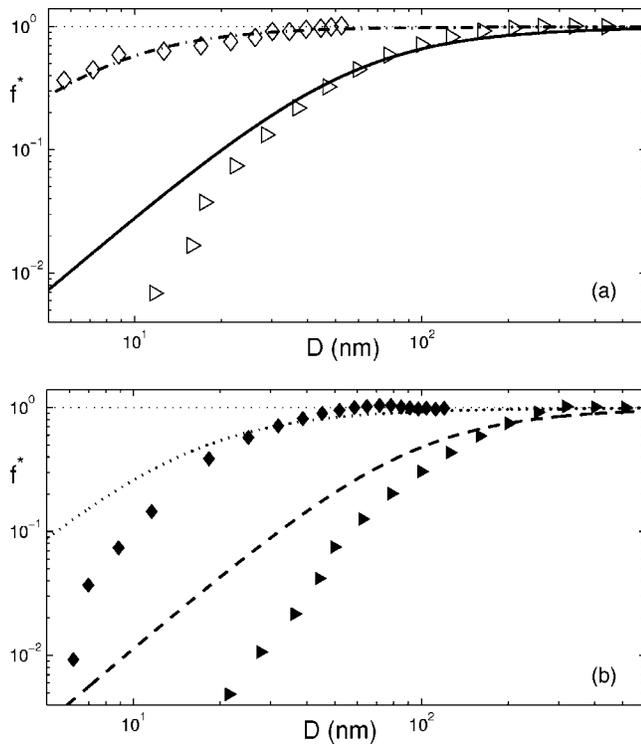
FIG. 2. A comparison between the experimental data of Zhu and Granick (2001) and the dynamic model (23) with $R_0 = 10$ nm and $\phi = 99\%$. (a) Small amplitude experimental data; ($\diamond$): measurements for $d = 0.5$ nm, $\omega = 1$ Hz; dashed-dotted line: model for $\theta = 177°$; ($\triangleright$): measurements for $d = 1.6$ nm, $\omega = 10$ Hz; solid line: model for $\theta = 132°$. (b) Large amplitude experimental data. ($\blacklozenge$): measurements for $d = 6$ nm, $\omega = 1$ Hz; dotted line: model for $\theta = 168°$; ($\blacktriangleright$): measurements for $d = 6$ nm, $\omega = 10$ Hz; dashed line: model for $\theta = 90°$.

mental results of [21–24] on the typical size, distribution, and morphology of bubbles observed by atomic force microscopy.

The "leaking mattress" model we have presented in the preceding sections has three free parameters which we fit to the experimental data: (a) the area fraction of the bubbles on the surface, $0 \leq \phi \leq 1$, (b) the size of the spherical bubbles, described by their radius of curvature R_0, and (c) the microscopic contact angle θ at the bubble level, which significantly differs from the macroscopic contact angle because of both intermolecular and electrical forces at the nanometer scale. Note that ϕ is related to the area fraction n by the formula $\phi = n\pi R_0^2 \sin^2 \theta$.

Furthermore, in order to present a meaningful fit to available data, we require that in each experiment, the two layers of bubbles fit in the gap between the sphere and the plane for all separation distance. This is a geometrical constraint written as $2h_0 = 2R_0(1 + \cos \theta) \leq \min(D)$ [45].

The model (23) can be well fit to the experiments [8] with appropriate parameter choices. The best fits are obtained when we choose $R_0 \approx 10$ nm. This is illustrated in Fig. 2 where the fits are compared the force ratio from the model to the small (a) and large (b) amplitude data from Zhu and Granick [8]; the values of the angles θ were chosen for each curve to be the best in a least-square sense and $\phi = 99\%$. As
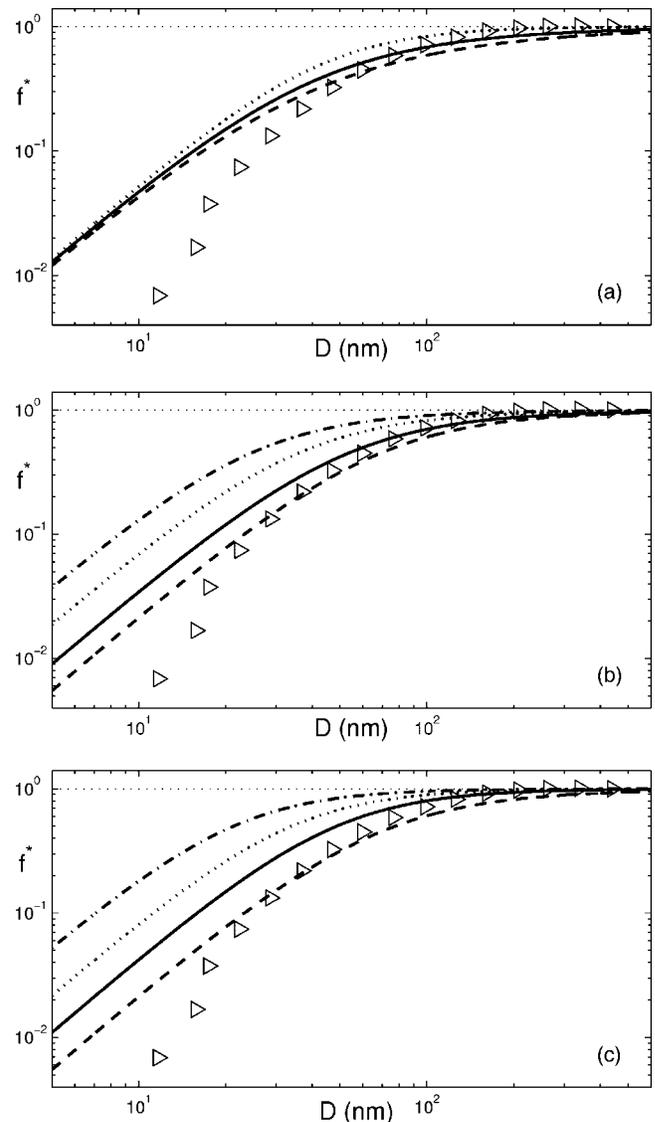

FIG. 3. A comparison between the experiment from Ref. [8] with $d = 1.6$ nm and $\omega = 10$ Hz ($\triangleright$) and the model for different bubble sizes, contact angles, and surface coverage. (a) Influence of bubble size; model with surface coverage $\phi = 0.99$, contact angle $\theta = 150°$, and bubble sizes $R_0 = 1$ nm (dotted line), 25 nm (solid line), and 50 nm (dashed line). (b) Influence of contact angle; model with surface coverage $\phi = 0.99$, bubble size $R_0 = 10$ nm, and contact angles $\theta = 120°$ (dashed line), 140° (solid line), 160° (dotted line), and 170° (dashed-dotted line). (c) Influence of surface coverage; model with bubble size $R_0 = 10$ nm, contact angle $\theta = 120°$, and surface coverage $\phi = 0.1$ (dashed-dotted line), $\phi = 0.25$ (dotted line), $\phi = 0.5$ (solid line), and $\phi = 0.99$ (dashed line).

expected from the linearity of our model, the fit to the low amplitude data of Ref. [8] is better than that obtained for oscillations of larger amplitude.

We explore the influence of the three parameters of our model (ϕ, R_0, θ) in Figs. 3(a)–3(c) for the measurements from Ref. [8] with $d = 1.6$ nm and $\omega = 10$ Hz.

We first find that the results of our model depend weakly on the bubble sizes: the results in Fig. 3(a) are consistent

with the experimental data for a large range of bubble sizes, $R_0 \sim 1 - 50$ nm. These sizes are in agreement with the experimental evidence of bubbles in Refs. [21–24], as summarized in Table I, although somewhat smaller. As a matter of comparison, the data in Ref. [23] show a large standard deviation (up to 70%) for the bubble area.

As a difference, we find that the results of our model depend on both the assumed microscopic contact angle θ and coverage of the surface by the bubbles ϕ. We observe variations in the contact angles leading to best fit to the four experiments (Fig. 2) and also note that we obtain a departure from the best fit when the angle is chosen to be significantly different [Fig. 3(b)]. In three out of four experiments, we find that the microscopic contact is larger than the macroscopic contact angle 110° characterizing the wetting of deionized water on the surfaces used in Ref. [8]. This result is consistent with the data in Table I where, in all cases, bubbles were found experimentally to be flat with microscopic contact angles larger than the macroscopic wetting angles. The fourth set of data from Ref. [8] is found to be consistent with a microscopic angle of about 90°. Although this is different from the data in [21–24], it is consistent with theoretical studies which show that intermolecular forces lead to microscopic contact angles that are always closer to 90° than their macroscopic counterpart [38]. Furthermore, we note that electrical effects are known to have significant impact on contact angles of bubbles and drops [39,40].

Finally, we find that our model is consistent with the experimental data when the surface coverage is assumed to be large and almost equal to 100% [see Fig. 3(c)]. This result compares well with the available data on bubbles where, in three out of four studies [22–24], the bubbles were found to cover almost entirely the solid surface. As a difference, the pictures in Ref. [21] show bubbles with lower surface coverage. We also note that our previous study of slip in pressure-driven flow experiments led to a similar conclusion: in order for surface-attached bubbles to be responsible for the measured effective slip, surface coverage of almost 100% was necessary [18].

IV. CONCLUSION

We have explored in this paper the consequences of the presence of nanobubbles on the surfaces where squeeze flow experiments are performed. We have shown that, within the framework of a simple stabilizing model, the time dynamics of bubbles always leads naturally to a shear-dependent decrease in the measured viscous force by a "leaking mattress" effect. The effect was found to increase with the viscosity of the fluid and the size of the sphere, in agreement with earlier experimental results.

We emphasize that this mechanism is of *dynamic* origin, and is not a consequence of the microscopic slip at the bubble surfaces; in particular, we argue that this is why shear-dependent slip lengths have not been reported by investigations of slip in pressure-driven flow experiments to date, where no oscillatory pressure is present to trigger an effect similar to the one proposed here. Also, the mechanism

we propose should also apply to squeeze flow experiments performed on superhydrophobic surfaces such those reported in Ref. [41] with small air bubbles trapped on fractal surfaces (see also Ref. [42]).

Assuming the presence of bubbles, the calculations on the model have been performed with several simplifying assumptions and, in particular, additional contributions to the sets of coefficients (k_1, k_2) could come from bridging bubbles, large amplitude oscillations of the solid sphere or bubble interactions, deformation, or displacement on the solid surface.

We have then presented a comparison between the results of our model and the experiments of Zhu and Granick. We found that our model gives results that are in agreement with the force decrease measured experimentally, for bubble features that are consistent with available experimental data on nanobubbles (bubble size $R_0 \sim 10$ nm, large microscopic contact angles, large surface coverage). Finally, a formula has been proposed for the (additional) effective elasticity provided by the bubbles to the solid surface.

We note that our study does not rule out the possibility of bubbles with dynamically selected sizes. It has been reported experimentally in Ref. [43] that the jump-in distance between two hydrophobic surfaces in water, believed to be due to the presence of bubbles, depended on the history of the sample; performing the experiment several times led to changes in the jump-in distances over time, which was found to remain constant only after a few periods. A similar scenario could be envisioned in experiments such as Ref. [8].

To conclude, we present a simple prediction based on the results of our model. If a squeeze flow experiment was performed with two different surfaces, say a hydrophobic plane and a hydrophilic sphere, force ratio measurements displaying shear-dependent results should be able to test whether the ideas put forward in this paper are valid. Indeed, if the force decreases were really due, not to bubbles, but to a change in the hydrodynamic boundary condition for flow past the hydrophobic surface, the maximum force decrease one could expect to obtain is 1/4 for the case of a perfectly slipping surface (see Ref. [33] for the calculation; this result can also be found by symmetry about the plane where slip occurs). If, alternatively, the measurements are due to a "leaking mattress" effect similar to the one we propose here, Eq. (6) should also apply (with different prefactors) and therefore so is Eq. (23); consequently, force ratio smaller than 1/4 should be obtained in this case. This proposition for an experiment, together with the prediction for the in-phase response of the force (24), would allow our model to be tested experimentally.

ACKNOWLEDGMENTS

[1] S. Goldstein, *Modern Developments in Fluid Dynamics* (Clarendon, Oxford, 1938), Vol. II, p. 676.

[2] Y. Zhu and S. Granick, Phys. Rev. Lett. **88**, 106102 (2002).

[3] K.M. Jansons, Phys. Fluids **31**, 15 (1988).

[4] S. Richardson, J. Fluid Mech. **59**, 707 (1973).

[5] R. Pit, H. Hervet, and L. Léger, Phys. Rev. Lett. **85**, 980 (2000).

[6] J. Baudry, E. Charlaix, A. Tonck, and D. Mazuyer, Langmuir **17**, 5232 (2001).

[7] V.S.J. Craig, C. Neto, and D.R.M. Williams, Phys. Rev. Lett. **87**, 054504 (2001).

[8] Y. Zhu and S. Granick, Phys. Rev. Lett. **87**, 096105 (2001).

[9] E. Bonaccurso, M. Kappl, and H.-J. Butt, Phys. Rev. Lett. **88**, 076103 (2002).

[10] J.-T. Cheng and N. Giordano, Phys. Rev. E **65**, 031206 (2002).

[11] D.C. Tretheway, and C.D. Meinhart, Phys. Fluids **14**, L9 (2002).

[12] C. Cottin-Bizonne, S. Jurine, J. Baudry, J. Crassous, F. Restagno, and E. Charlaix, Eur. Phys. J. E **9**, 47 (2002).

[13] P.A. Thompson and S.M. Troian, Nature (London) **389**, 360 (1997).

[14] J.-L. Barrat and L. Bocquet, Phys. Rev. Lett. **82**, 4671 (1999).

[15] H. Brenner and V. Ganesan, Phys. Rev. E **61**, 6879 (2000).

[16] M. Cieplak, J. Koplik, and J.R. Banavar, Phys. Rev. Lett. **86**, 803 (2001).

[17] C. Denniston and M.O. Robbins, Phys. Rev. Lett. **87**, 178302 (2001).

[18] E. Lauga and H.A. Stone, J. Fluid Mech. **489**, 55 (2003).

[19] P.G. de Gennes, Langmuir **18**, 3413 (2002).

[20] C.L.M.H. Navier, *Mémoires de l'Académie Royale des Sciences de l'Institut de France* **VI**, 389 (1823).

[21] N. Ishida, T. Inoue, M. Miyahara, and K. Higashitani, Langmuir **16**, 6377 (2000).

[22] J.W.G. Tyrrell and P. Attard, Phys. Rev. Lett. **87**, 176104 (2001).

[23] J.W.G. Tyrrell and P. Attard, Langmuir **18**, 160 (2002).

[24] R. Steitz, T. Gutberlet, T. Hauss, B. Klösgen, R. Krastev, S. Schemmel, A.C. Simonsen, and G.H. Findenegg, Langmuir **19**, 2409 (2003).

[25] J. Israelachvili, *Intermolecular and Surface Forces* (Academic, New York, 1992).

[26] A. Carambassis, L.C. Jonker, P. Attard, and M.W. Rutland, Phys. Rev. Lett. **80**, 5357 (1998).

[27] J. Mahnke, J. Stearnes, R.A. Hayes, D. Fornasiero, and J. Ralston, Phys. Chem. Chem. Phys. **1**, 2793 (1999).

[28] P. Attard, Langmuir **16**, 4455 (2000).

[29] G.E. Yakubov, H.-S. Butt, and O.I. Vinogradova, J. Phys. Chem. B **104**, 3407 (2000).

[30] E. Schnell, J. Appl. Phys. **27**, 1149 (1956).

[31] N.V. Churaev, V.D. Sobolev, and A.N. Somov, J. Colloid Interface Sci. **97**, 574 (1984).

[32] K. Watanabe, Y. Udagawa, and H. Udagawa, J. Fluid Mech. **381**, 225 (1999).

[33] O.I. Vinogradova, Langmuir **11**, 2213 (1995).

[34] S. Ljunggren and J.C. Eriksson, Colloids Surf., A **129–130**, 151 (1997).

[35] P. Attard, Physica A **314**, 696 (2002).

[36] J.R. Philip, Z. Angew. Math. Phys. **23**, 353 (1972).

[37] G.I. Taylor, Proc. R. Soc. London, Ser. A **219**, 186 (1953).

[38] L.M. Hocking, Phys. Fluids A **5**, 793 (1993).

[39] C. Quilliet and B. Berge, Curr. Opin. Colloid Interface Sci. **6**, 34 (2001).

[40] T. Chou, Phys. Rev. Lett. **87**, 106101 (2001).

[41] T. Onda, S. Shibuichi, N. Satoh, and K. Tsuji, Langmuir **12**, 2125 (1996).

[42] J. Bico, C. Marzolin, and D. Quéré, Europhys. Lett. **47**, 220 (1999).

[43] G.E. Yakubov, H.-J. Butt, and O.I. Vinogradova, J. Phys. Chem. B **104**, 3407 (2000).

[44] The general solution to Eq. (20) also has an exponentially decaying transient occurring on a time scale $\tau \sim \delta k_2/(1+\delta k_1)$ with $\tau \sim 1$ ms or less in experiments such as [8].

[45] The model also requires specification of the effective slip length λ in Eq. (3). Since a set of gas bubbles on a surface resists fluid motion more strongly than a gas layer, Eq. (1) is not appropriate. We have experimented with several models (see, e.g., [18,36]), all of which give slip length in the range ($\lambda \sim 10-100$ nm depending on the experiment). Owing to the weak dependence of f^* on the slip length, the precise value of λ has virtually no impact on the quantitative results of our fits.